Deformation Matching: Force Computation based on Deformation Optimization*

Koichi Hirota, Yusuke Ujitoko, Sho Sakurai, Takuya Nojima, *Member, IEEE*

***Abstract*—The tactile information to be presented to a user during interaction with a virtual object is calculated by simulating the contact between the object model and user model. In the simulation, a distributed force is applied to the contact area on the skin tissue of users' hands and results in deformation of the skin tissue. The skin deformation caused by the distributed force is the target contact state that should be presented by the device. However, most multipoint haptic displays do not have sufficient degrees of freedom (DoF) to represent the target contact state. This paper presents the concept and formulation of "deformation matching," whereby the output force is calculated to minimize the error between the target skin deformation and skin deformation that can be realized by the limited DoF device's output force. For comparison, the conventional concept of "force matching" was also formulated. The difference in human perception between these two concepts in the expression of friction was investigated through experiments using a pin-array tactile display capable of stimulating 128 points. It was demonstrated that the perception of the friction coefficient was more sensitive and the perception of the friction direction was more accurate in deformation matching than in force matching.**

***Index Terms*—Haptic interface, Haptic rendering, Tactile display, Virtual reality.**

I. Introduction

Increasing the degrees of freedom (DoF) and presenting distributed stimuli is a development trend of haptic devices. It is expected that increased DoF will make it possible to convey the local shape and surface properties of the object. Tactile sense is a measurement system that is capable of receiving distributed stimuli on the skin surface, and haptic devices need to have sufficient spatial resolution and DoF for the properties of such receptors. Fingertips are known to have particularly high tactile resolution, and tactile displays that exert force on multiple points, hereinafter referred to as multipoint tactile displays, have been developed.

The tactile information to be presented to the user during interaction with a virtual object is calculated by simulating the contact between the object model and user model. Fingers and hands have flexible tissue on the surface, which exerts a distributed force on the contact area with an object and resulting in the deformation of the tissue. This corresponds to the target contact state that is presented by the device. The DoFs of the calculated tactile information vary depending on the model approximation degree. When the DoF of the simulation and device are equivalent, it is possible for the device to present the target contact state as it is. However, if the DoF differ, it is necessary to calculate a suitable output adaptively for the limited DoF device to realize the target contact state.

The aim of this study was to establish a haptic rendering algorithm that calculates the output force of a multipoint tactile display from the target contact state. The majority of studies on multipoint tactile displays have focused on device implementation, and the evaluation of such devices has been performed by focusing on the benefits derived from the density of the stimuli, such as improvement in the recognition of fine two-dimensional patterns [1, 2, 3, 4].

We previously attempted to present the contact force by using a pin-array tactile display, by approximately mapping the force to closely located pins. However, in the preliminary experiment, it appeared that it was difficult to provide a sufficient sense of reality. One of the reasons for this is that the rendering method that maps the force to the pin cannot sufficiently reproduce the deformed state of the skin.

Recently, Perez et al. proposed the concept of 'optimization-based haptic rendering' [5], which formulates the calculation of the device output as an optimization problem that minimizes the error between the target deformation and the deformation expected to be caused by the device output. In this pioneering work, an approach for minimizing skin deformation error has been presented and demonstrated. In subsequent research, an extension of the approach to optimization regarding skin stress has been investigated [6]. However, their work only addressed the 3 DoF device and did not address the higher DoF device.

In the current study, we focus on the deformation, rather than force, of the skin contact state. We propose a rendering method based on the concept of minimizing the error between the displacement of the target deformation and that of the skin caused by the device. The device output force is calculated by solving an optimization problem that considers the device constraints. This approach is referred to as "deformation matching" in this study.

The contributions of this study are the formulation of

Submitted for review on April 11, 2021.

This work was supported by JSPS KAKENHI (Grant Number JP17H00754). In part, this research used the ADVENTURE System from the University of Tokyo. Moreover, this work was performed using body geometry data from the BodyParts3D database provided by the National Bioscience Database Center.

K. Hirota is with the University of Electro-Communications, Chōfu, Tokyo 182-8585, Japan (e-mail: hirota@vogue.is.uec.ac.jp).

Y. Ujitoko is with NTT Communication Science Laboratories, Atsugi, Kanagawa 243-0198, Japan (e-mail: yusuke.ujitoko@gmail.com).

S. Sakurai is with the University of Electro-Communications, Chōfu, Tokyo 182-8585, Japan (e-mail: sho@vogue.is.uec.ac.jp).

T. Nojima is with the University of Electro-Communications, Chōfu, Tokyo 182-8585, Japan (e-mail: tnojima@nojilab.org).

deformation matching and the evaluation of the effectiveness of the approach through experiments using subjects. In the formulation, it is assumed that the relationship between the force and skin displacement can be expressed by a deformation model. Moreover, it is assumed that the device applies force, rather than displacement, on the skin. Although the nonlinearity associated with skin deformation has been noted in past studies [7], a linear model is used as the first step owing to the stability of convergence, as described below. Furthermore, as a comparative approach for the proposed method, we formulate the idea of minimizing the error between the target force and acting force of the device, hereinafter referred to as "force matching." This method is considered to be a generalization of the conventional method of calculating the device output by distributing the target force to nearby pins. In the evaluation using subjects, the effectiveness of the proposed method for the presentation of frictional force is verified by means of a pin-array-type tactile display that exerts forces on the skin through pins. The presentation of frictional forces is a common tactile expression and is also important in applications; however, it is a challenging task for pin-array devices that can only exert force in a direction that is approximately perpendicular to the skin. We attempt to reproduce the deformation of the finger when friction is applied by deformation matching.

The following section describes related research and clarifies the focus of our study. The formulations of the deformation matching and force matching are presented in Section III, and the implementation thereof for the experiments is described in Section IV. The conditions and procedures of the experiments are detailed in Section V, and the results are discussed in Section VI. Finally, Section VII summarizes the results of the study and outlines future issues.

II. Related Research

A. Haptic Devices

The need for haptic feedback was noted in the early stages of research on tele-robotics and virtual reality (VR), and various implementation methods have been proposed. These methods can be categorized into three typical approaches. The first is an approach that expresses the force acting on a tool. Many commercial haptic devices (e.g., PHANToM with pen grips and Falcon) are based on this method. The second is an approach that expresses the object itself or its properties. This method provides the reality of an object by expressing values such as the object shape, the forces associated with the operation (e.g., movement, inertia, and vibration), and surface properties (e.g., friction and smoothness). The third is an approach that expresses the tactile stimulus on the skin surface of the user. This method creates a tactile experience by presenting the forces and displacements on the skin surface.

Various stimulus types have been investigated to express tactile stimuli on the skin surface of the user. The fundamental approach involves presenting the force. The original PHANToM presented a force vector to a finger via a gimbal and thimble [8]. Moreover, the presentation of forces with two DoFs (i.e., compression and shear) by using a wearable device has been investigated [9]. Methods that densely integrate actuators have been developed to present a distributed force on the skin. Furthermore, the use of gel materials [10], solenoids [11], flexible tendons [1], shape memory alloys (SMAs) [12], and pneumatics [2] has been proposed.

Another fundamental approach is the application of skin deformation. This method approximates the deformed shape with a plane [13] and attempts to increase the DoF to improve deformation accuracy [3, 4]. Skin stretch is another concept that is similar to the approach of applying deformation to the skin. It has been demonstrated that it is possible to present torque to the palm [14], present action force to the fingers [15], and express softness [16]. The application of vibration stimulation to the presentation of two-dimensional patterns such as characters has been studied for a long time [17], and in recent years, the application to texture expression in VR [18] has also been studied. Electrical stimulation is a method of electrical action upon mechanoreceptors and nerves. A method has been developed for selectively stimulating the receptors by controlling an electrode array [19], which is expected to be applied to general presentations such as pressure and vibration.

B. Haptic Rendering

In addition to the device, the calculation process of haptic information is indispensable for haptic feedback. This process is known as haptic rendering. According to Salisbury, "haptic rendering is the process of computing and generating forces in response to user interactions with virtual objects" [20]. Early haptic rendering research investigated models for user–object interaction through points of action, and in this context, God object methods [21] as well as shape and texture representation methods [22, 23] have been proposed. Subsequently, a model that approximates the surface contact by the skin was examined based on the demand for the reality of the gripping operation by the finger or hand. Moreover, an approximate deformation model by a spherical surface [24], an approximate calculation of the contact area [25], a reaction force calculation by skinning [26], and aggregation of constraints by contact [27] have been proposed. In recent years, techniques for physically computing the skin deformation have been investigated, and the introduction of locally deformable pads into finger models [28] and interactions with deformable models of the entire hand [29, 30] have been studied. Furthermore, it has been noted that tissue nonlinearity needs to be introduced for more accurate contact state calculations [7].

Owing to increasing DoF and complexity of haptic devices, the relationship between the target contact state and the contact state presented by the device has become less trivial. Therefore, a method of mapping from the former to the latter is required. Sato et al. proposed and verified the concept of calculating the electrical stimulation from the strain energy density associated with the tissue deformation resulting from contact for the presentation of electrical tactile stimulation [31]. As described later, the firing frequency of the receptor is proportional to the strain energy density. Maemori et al. also proposed a method to control the suction display by using strain energy density as an index [32].

In general, the contact state on the skin is not necessarily directly controllable depending on the configuration of the device. In such cases, the device output that will realize or approximate the target state must be estimated based on a model that relates the device output with the contact state. Hence, the estimation can be formulated as a problem for finding the device output that minimizes the error in the contact state using the model. Such approaches are categorized as "optimization-based haptic rendering".

A pioneering work has been done by Perez et al. in which they proposed a method for calculating device configuration in the presentation of a plane to a finger using a thimble tactile device [5]. This technique was formulated as an optimization problem that minimized the difference between the target skin displacement and the displacement caused by the device on the skin with postural constraints of the device. Verschoor et al. proposed and evaluated a method for matching the stress generated by the device on the skin with the target stress for a thimble tactile device [6]. The stress caused by the device was estimated using a skin deformation model. In this method, the friction state was estimated considering the dependence on the device operation trajectory, and a neural network was used for the calculation to obtain the stress distribution from the device configuration and friction state.

Another research applies the concept of optimization-based haptic rendering to the presentation of distributed pressure using a mid-air ultrasound device. This research proposed and evaluated algorithms for finding an optimal path of the stimulation under constraints due to the physical characteristics of the device and temporal resolution of tactile perception [33, 34].

C. Tactile Perception

A typical receptive property of mechanical tactile stimuli is the tactile two-point threshold, which allows humans to distinguish between two points on the skin when they are stimulated simultaneously [35]. The tactile two-point threshold is often described as an indicator of the spatial resolution that is required for tactile displays. In fact, it has been noted that recognition with a spatial resolution higher than the tactile two-point threshold is possible [36, 37]. Regarding the perception of tactile stimulus movement, it has been demonstrated that the inter-stimulus onset interval and duration affect the occurrence of tactile apparent motion [38]. This suggests that it is necessary to increase the stimulation density in the expression of smooth tactile movement.

Furthermore, research is currently being conducted to elucidate the perception of tactile sensation from a mechanical perspective. Tactile receptor response properties have been revealed to be consistent with strain energy density-based models [39]. Moreover, it has been demonstrated that the placement of receptors on the skin is consistent with the properties of the receptors [40]. The illusion that skin suction produces a sensation that is similar to skin compression has also been reported. This illusion can be explained by the similarity of the strain energy densities between suction and compression in the tissues near the receptors [41].

D. Focus of this Study

According to the above review, a high-density and multi-DoF device is required to express the stimulus acting on the skin accurately. However, a haptic rendering method for such a device that considers the DoF of the actuator and the restriction of the operation has not yet been established.

In this study, we propose a rendering method for a tactile device that presents the force on multiple points on the skin. The fundamental concept is the optimization of the device output force based on the error of the skin deformation by the device from the target deformation. The minimization of the skin deformation error was also proposed in the study by Perez et al. [5], but their study focused on thimble tactile devices, and the formulation of a multipoint tactile display was not discussed.

In this study, we prioritized computational stability, because this work is a preliminary attempt at rendering multipoint tactile displays. As an optimization index, optimization based on the strain energy density near the sensory receptor, instead of the deformation, was an option, but it was not adopted in this study. This is because the illusion of suction [41] suggests that this optimization problem may have multiple local solutions. The nonlinearity of skin deformation was also not introduced owing to concerns that it would degrade the convergence of the optimization calculations. Furthermore, this study employed a pin array device that was previously developed in the laboratory for evaluation, and in this sense, the results described below is specific to the device.

III. Problem Formulation

In this section, the deformation matching and force matching approaches are formulated. Deformation matching and force matching are two different methods for calculating the device output to minimize displacement and force errors, respectively, from the target deformation state.

A. Deformation Matching

Suppose that the relationship between the skin force f and displacement u can be calculated by the skin deformation model as $f = K(u)$. Furthermore, it is assumed that the force generated on the skin by the device action f_d can be calculated using a device model as $f^* = A(f_d)$. The deformation u^* due to the device action is expressed as follows:

$$u^* = K^{-1}(f^*) = K^{-1}\big(A(f_d)\big). \quad (1)$$

Deformation matching is the problem of determining f_d to satisfy the following:

$$\|u - u^*\|^2 \rightarrow min. \quad (2)$$

In the following, the formulation of a linear model is discussed. A model of skin deformation by the linear FEM is generally defined as follows [42]: The subscript c indicates the DoF with fixed (or imposed displacement) boundary conditions. For a given u_c and f, u and f_c are calculated.

$$\begin{pmatrix} f \\ f_c \end{pmatrix} = \begin{pmatrix} K_0 & K_1 \\ K_2 & K_3 \end{pmatrix} \begin{pmatrix} u \\ u_c \end{pmatrix}. \quad (3)$$

The device is operated by actuators (e.g., voice coil motors) and presents an output force on the skin. The driving force of the actuators is converted into an output force through a transmitting mechanism that depends on the device. In the following, we consider the case in which a linear relationship exists between the driving force and the force acting on the skin. Assuming that a device with n_d DoF operates with a driving force f_d ($n_d \times 1$) to generate a force f^* on the skin, the relationship between the two can be described as follows:

$$f^* = Af_d. \tag{4}$$

In the pin-array device used in the experiment described later, the acting force acts directly on the skin, without requiring a transmission mechanism, and the direction is limited to the pin driving direction. Moreover, because the point of action of the pin and the model node do not always match, it is necessary to associate the acting force of the pin with the neighboring nodes according to the position of the point of action. Considering the features of a pin-array tactile display, A is defined as the product of A_d and A_p ($A = A_d A_p$), where A_p ($3n_d \times n_d$) is a matrix in which the vectors of the pin action directions are arranged, and A_d ($3n \times 3n_d$) is a matrix of coefficients that distribute the force of the pins to the model nodes.

In a linear model, the displacement u^* due to the device action f_d is calculated by

$$u^* = {K_0}^{-1}Af_d. \tag{5}$$

Let us consider the determination of f_d that minimizes the deformation error $\|u - u^*\|^2$ for a given target displacement u.

$$\|u - u^*\|^2 = \left\|u - {K_0}^{-1}Af_d\right\|^2 \to min. \tag{6}$$

Note that the model nodes are not necessarily arranged in a spatially even density. That is, the error defined by the equation can be considered as an index that is weighted by the spatial density of the nodes.

In the following, we define L as ${K_0}^{-1}A \equiv L$ ($3n \times n_d$).

$$\begin{aligned}\|u - u^*\|^2 &= (u - Lf_d)^T(u - Lf_d)\\ &= u^T u - (Lf_d)^T u - u^T(Lf_d) + (Lf_d)^T(Lf_d)\\ &= u^T u - 2u^T Lf_d + {f_d}^T L^T Lf_d.\end{aligned} \tag{7}$$

Because the target displacement u is a fixed value, $u^T u$ is a constant term, and thus, the following minimization problem arises:

$${f_d}^T L^T Lf_d - 2u^T Lf_d \to min. \tag{8}$$

In this case, because $x^T L^T Lx = (Lx)^T Lx \geq 0$, $L^T L$ is a semipositive definite matrix. In reality, in a device without a control state where $u^* = 0$ for $f_d \neq 0$, $L^T L$ becomes a definite matrix, and the above problem becomes a convex quadratic programming problem [43]. In the unconstrained case, this solution is provided using L^+, which is the pseudo-inverse matrix of L. This solution is referred to as DM0.

$$f_d = L^+ u. \tag{9}$$

In many multipoint tactile displays, the point of action (or pin) and skin do not adhere to one another, and a force cannot be exerted in the skin pulling direction. The pin-array device used in the experiments described below has similar restrictions because air pressure cannot be controlled by negative pressure. This constraint is expressed in the following form:

$${f_d}_i \geq 0 \ \ (i = 1, \cdots, n). \tag{10}$$

A straightforward means of introducing this constraint is to clamp the above solution (DM0) to 0. This solution is referred to as DM1.

$${f_d}_i \leftarrow \max\left({f_d}_i, 0\right). \tag{11}$$

It is necessary to consider optimization under constraints to obtain a more precise solution. The necessary and sufficient condition for the optimality of the conditional convex quadratic programming problem is known as the Karush–Kuhn–Tucker (KKT) condition. The KKT condition in the above problem is expressed as follows by using the Lagrange variable λ ($n_d \times 1$). This solution is referred to as DM2.

$$\begin{cases} 2L^T Lf_d - 2L^T u = \lambda \\ \lambda_i {f_d}_i = 0 \\ {f_d}_i \geq 0 \\ \lambda_i \geq 0 \end{cases} \quad (i = 1, \cdots, n). \tag{12}$$

B. Force Matching

As an approach for comparing the proposed methods in the previous subsection, we also formulate a conventional presentation method focusing on force. The majority of research on multipoint tactile displays has focused on the device, with few discussions on the calculation algorithm of the output force. The general concept in this research context is to reproduce the calculated force on the device. This concept can be generalized as force-based optimization; that is, the problem of determining f_d that minimizes the error between the target force f and force f^* owing to the device action.

$$\|f - f^*\|^2 = \|f - Af_d\|^2 \to min. \tag{13}$$

As with DM0, the error defined by $\|f - f^*\|^2$ is an index that is weighted by the density of the nodes. Moreover, in this definition, all the nodes are subject to calculation. The sum of the forces of the nodes that are not in contact with the object or on which no external force acts calculated by the FEM is 0. Therefore, this definition only considers the acting force of the nodes that are in contact with the object.

The formula for the force error is expanded as follows:

$$\begin{aligned}\|f - f^*\|^2 &= (f - Af_d)^T(f - Af_d)\\ &= f^T f - 2f^T Af_d + {f_d}^T A^T Af_d.\end{aligned} \tag{14}$$

In the above, because the target force f is a fixed value, $f^T f$ is a constant term. Thus, the following minimization problem can be obtained:

$${f_d}^T A^T Af_d - 2f^T Af_d \to min, \tag{15}$$

where $A^T A$ is a definite matrix; hence, minimization is solved as a convex quadratic programming problem. This solution, without constraints, is obtained using A^+, which is the pseudo-inverse matrix of A. This solution is referred to as FM0.

$$f_d = A^+ f. \tag{16}$$

An easy means of considering the constraints of the force feedback device is to clamp the above solution (FM0) to 0. This solution is referred to as FM1.

$${f_d}_i \leftarrow \max\left({f_d}_i, 0\right). \tag{17}$$

It is necessary to consider optimization under the constraints to obtain a more precise solution. The KKT condition of this problem is expressed as follows, using the Lagrange variable λ ($n_d \times 1$). This solution is referred to as FM2.

$$\begin{cases} 2A^T A f_d - 2A^T u = \lambda \\ \lambda_i f_{d_i} = 0 \\ f_{d_i} \geq 0 \\ \lambda_i \geq 0 \end{cases} \quad (i = 1, \cdots, n). \tag{18}$$

IV. Experimental Setup

The experiment focused on the expression of friction when the finger touched a plane and the plane moved relative to the finger. The rendering calculations were performed in two steps. The first step was a contact simulation, which calculated the deformation of the finger and the force acting on the contact area due to frictional contact. This was the target contact state in the subsequent matching process. In the second step, the device acting force was calculated by solving the optimization problem by means of deformation matching and force matching, as discussed in Section III. The same finger model was used for both the contact simulation and matching. A pin-array device that presented a pressure sensation at 128 points was used as a force feedback device. Both the contact simulation and matching were performed offline to generate time-series data for the device output. In the experiment, the force was presented to the subject by driving the device based on these data.

A. Simulation Model

The finger model represented soft tissue in the area beyond the center of the intermediate phalanx (Fig. 1). The basic model shape was obtained by cutting out a bone and skin shaped model of the finger part from a body model database (BodyParts3d [44]). A tetrahedral mesh was generated for this shape using the TetMesh program (ADVENTURE project [45]). Fixed boundary conditions were set for the nodes on the surface that contacted the bones and nail. The mesh consisted of 27,737 tetrahedrons and 5,800 nodes, and the number of free nodes (n) was 4,435. The material was uniform in the mesh, the Young's modulus was $E_0 = 1.0 \times 10^5$ Pa, and the Poisson's ratio was $\nu = 0.48$. The Young's modulus was adjusted at the time of presentation by using the calibration method described later.

In the contact simulation, the frictional force was generated by the relative movement of the plane in contact with the finger. In the initial state (time $t = 0$), the finger was pressed against the plane at a certain depth d. The simulation was performed under four different conditions with d values of 0.5, 1.0, 1.5, and 2.0 mm. Over time, the plane underwent tangential displacement l, as defined by the following function:

$$l = -R\cos(\omega t). \tag{19}$$

In the above, the constant of the stroke is $R = 0.02$ m and the angular velocity is $\omega = \pi/4$ rad/s. That is, the plane reciprocates from a displacement of -0.02 m to 0.02 m with a period of 8 s. The initial contact state at $t = 0$ was calculated by applying normal displacement of the surface and then waiting for 100 simulation steps or 0.42 s for the simulation to become stable. The frictional force acting on the finger was stable and unchanging shortly after the entire contact area started to slip. In the experiment described later, it was assumed that a force was presented for 2 s from the start of the tangential motion.

B. Device Model

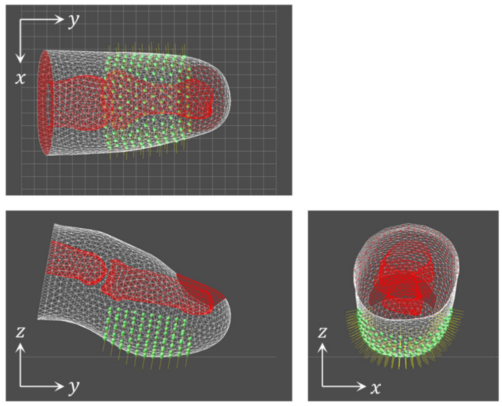

Figure 1. Mesh model for contact simulation and matching. The soft tissue in the area beyond the center of the intermediate phalanx was represented by a tetrahedral mesh model. A fixed boundary condition was implemented on the surfaces of the bones and nail, which is represented by the red mesh. The pin-array tactile display was assumed to be mounted on the finger at a small pitch angle. The points of action and lines of motion of the pins are represented by the green dots and yellow lines, respectively.

Figure 2. High-density pin-array haptic display. The device has 128 pins, the output force of which is controlled independently.

The experiment used a pin-array tactile display (see [2] for details). The device had 128 contact pins, and their output force was controlled independently. The pins were driven pneumatically, and the pin pitch was approximately 1.5 mm. The pins were arranged on a cylindrical surface, and the driving direction was toward the axis of the cylindrical surface (Fig. 2). The pin stroke is approximately 5 mm, the maximum force is 0.4 N, and the control delay is approximately 75 ms. The weight of the device is almost balanced by the rubber band suspension, and the device is fixed to the finger by pressing the back of the finger with a velcro fastener. The point of action of each pin on the mesh model was calculated as the intersection of the pin motion axis and the model surface without deformation when the device was attached to the finger pad. The direction of the force action by the pin was assumed to be equal to the direction of the pin operating axis (green dots and yellow lines, respectively, in Fig. 1). In practice, the finger and pin may slide in a direction orthogonal to the motion axis; however, in the model in this study, it was assumed that the point of action did not change. Similarly, the friction between the pin and finger may generate a force in the direction orthogonal to the movement; however, this was also not considered.

As mentioned in Section III.A, A_p ($3n_d \times n_d$) was constructed by arranging the vectors in the motion axis direction of the pin. A_d ($3n \times 3n_d$) defines the weight of the distribution of the acting force for all combinations of pins and model nodes. In this study, we assumed that the action of the

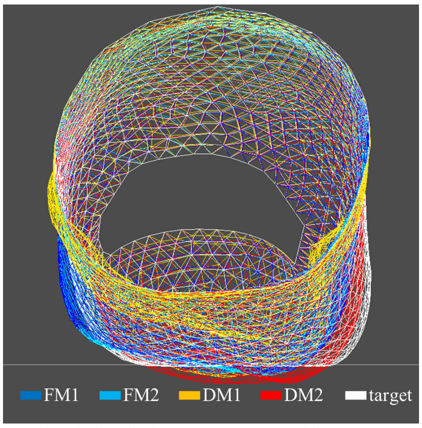

Figure 3. Example of skin deformation expected by FM1, FM2, DM1, and DM2 algorithms ($d = 2.0$ mm, $\mu = 0.6$). The target deformation was computed by the contact simulation.

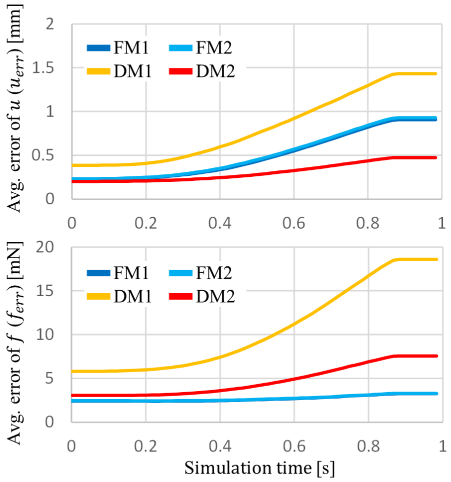

Figure 4. Example of average deformation and force errors (u_{err} and f_{err}, respectively) in progress of time ($d = 2.0$ mm, $\mu = 0.6$). The contact state became stable before approximately 1 s. The difference in the errors between FM1 and FM2 was relatively small, whereas the difference between DM1 and DM2 was remarkable.

pins is distributed to the surface of the model by a Gaussian distribution. On this basis, the Gaussian function values of all neighboring nodes were calculated for each pin, and the weight was calculated by dividing them by the sum. This method ensured that the sum of the forces acting on the neighboring nodes was consistent with that of the forces exerted by the pins. The distribution of the Gaussian function was empirically set to $\sigma = 0.8$ mm, considering the pin radius (0.5 mm) and internode distance (approximately 1 mm).

C. *Simulation and Matching*

The force acting on the finger and deformation of the finger owing to the contact were calculated using the static linear FEM. Friction contact with a flat surface was introduced using the penalty method. Coulomb's law was assumed for the friction model. That is, the node that was in contact with the plane was either in a static friction state or a dynamic friction state. The transition from the static friction state to the dynamic friction state occurred when the friction limit was exceeded, and the transition from the dynamic friction state to the static friction state occurred because of a stall in the friction speed. The time step of the calculation was 4.17 ms (i.e., 240 steps/s). This time interval may not necessarily be sufficient for the accurate reproduction of the transient state, but it is expected to be sufficient for the calculation of the friction state following the transition to a stable dynamic friction.

The device output f_d was calculated using the method described in Section III for the target states (i.e., f and u) that were obtained by the simulation. As an example, the deformations due to FM1, FM2, DM1, and DM2 at$d = 2.0$ mm and $\mu = 0.6$ are presented in Fig. 3, and their errors are depicted in Fig. 4. In FM2 and DM2, the optimization problem with inequality constraints was solved by using the interior point method. The average errors of the displacement and force in Fig. 4 were obtained as follows:

$$u_{err} = \sqrt{\|u - u^*\|^2/n}, \quad (20)$$

$$f_{err} = \sqrt{\|f - f^*\|^2/n}. \quad (21)$$

The target deformation is constrained by the contact surface, while the expected deformations by FM1, FM2, DM1, and DM2 can cause deformation that extends beyond the surface because the constraints by the surface are not imposed on the matching algorithms. The calculation results clarified that the difference between FM1 and FM2 was relatively small, the difference between DM1 and DM2 was remarkable, and DM1 exhibited a large error compared to the other methods. In DM1, a solution containing a large negative force was obtained in the unconstrained deformation matching and a large error was caused by clamping this negative force. In the example illustrated in Fig. 3, the deformation by DM2 appeared to be the closest to the target compared to those of the other algorithms. Based on this result, FM1 and DM2 were used for the comparison in the experiments. FM2 was not used because the difference from FM1 was relatively small and it could not be considered as a generalization of the conventional method. Moreover, DM1 was considered as unsuitable for comparison because of its large error.

D. *Calibration of Elasticity Constant*

Individual differences in the Young's modulus of the soft tissue of the fingers were considered by multiplying the target force by a constant. In the static deformation calculation by the linear FEM, the stiffness matrix K was a constant matrix proportional to the Young's modulus. In the contact simulation, the Young's modulus was assumed to be $E_0 = 1 \times 10^5$ Pa. When the actual Young's modulus of the subject was E, the stiffness matrix was E/E_0 times, and the force generated for the same deformation was also E/E_0 times. To estimate the Young's modulus of the user, the force against the compression deformation of the finger was measured and the ratio of this force to that of the contact simulation was calculated. This ratio was expected to approximate E/E_0. The device depicted in Fig. 5 was used for the measurements.

The measurements were performed according to the following procedure. The user maintained their finger lifted so that the finger touched the push plate lightly. The experimenter pushed their finger down on the stage and moved it until it touched the electronic scale. The stage was lowered by 0.5, 1.0, 1.5, and 2.0 mm from the contact state and the respective loads were read. Subsequently, α that minimized the sum of squares of the error between α times the load and the force by simulation was determined. In the experiment, the output force was calculated using the α value obtained for each subject. Fig. 6 presents the measurement results for each subject. The obtained value of α ranged from 0.61 to 0.90, depending on the subject.

V. EXPERIMENT

Two experiments were conducted. In Experiment 1, the perception of the tangential and normal forces (forces on the x–z plane in Fig. 1) when friction was applied to the fingers in only two directions (left or right) was investigated. In Experiment 2, the perception of the tangential force (force on the x–y plane in Fig. 1) owing to friction in any direction of the plane was investigated.

A. *Experiment 1: Frictional Force*

Subjects were presented the stimuli with a duration of 2 s calculated by the simulation and matching in section IV.A. The subjects were instructed to provide feedback on the direction and intensity of the perceived force in the $x-z$ plane. Each subject performed 112 trials, which included the following combinations for the contact simulation conditions: depth d (0.5, 1.0, 1.5, and 2.0 mm; four ways), coefficient of friction μ (0.0 to 0.6 in 0.1 increments; seven ways), friction direction (right/left; two ways), calculation algorithm (FM1/DM2; two ways), and one iteration. A within-subject design was adopted in which each subject evaluated all the conditions. The presentation order was randomized to reduce order effects. Fig. 7 depicts the target deformation u and expected deformation u^*

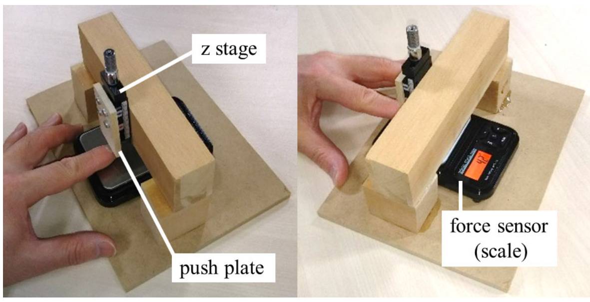

Figure 5. Homemade device for elasticity measurement. The device was composed of a stage and scale. The elasticity constant for each subject was obtained by measuring the force–displacement relationship and fitting the simulation data to the relationship.

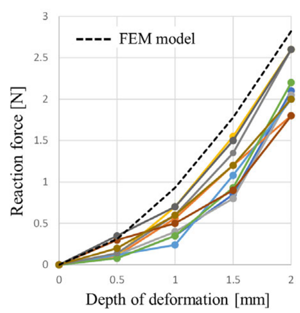

Figure 6. Force–displacement relationship measured for all subjects. The slope of the curve differed depending on the subject and the resulting factor α varied from 0.61 to 0.90.

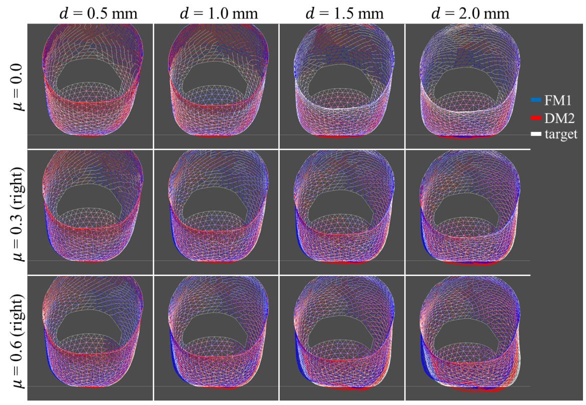

Figure 7. Examples of target and expected deformations of skin in Experiment 1. The deformation differed depending on the depth of contact d, friction coefficient μ.

for FM1 and DM2 under certain conditions, all of which were in the state of 2 s from the start of deformation. The subject provided feedback on the perceived force vector on the $x-z$ plane by pointing the mouse on the screen. The criteria for the force intensity were decided by the subjects. For convenience of providing feedback, a circle centered on the origin of the vector was displayed on the answering screen.

B. *Experiment 2: Direction of Frictional Force*

Subjects were presented the stimuli with a duration of 2 s calculated by the simulation and matching in Section IV.A. The subjects were instructed to provide feedback on the direction and intensity of the perceived force in the $x-y$ plane. Each subject performed 144 trials, which included the following combination of contact simulation conditions: depth d (2.0 mm; one way), coefficient of friction μ (0.5; one way), friction direction θ (360° in 10° steps; 36 ways), calculation algorithm (FM1/DM2; two ways), and two iterations. A within-subject design was adopted in which each subject evaluated all the conditions. The presentation order was randomized to reduce order effects. Fig. 8 presents the target deformation u and expected deformation u^* for FM1 and DM2 under certain conditions, all of which were in the state of 2 s from the start of deformation. The subjects provided feedback on the perceived force vector on the $x-y$ plane by pointing the mouse on the

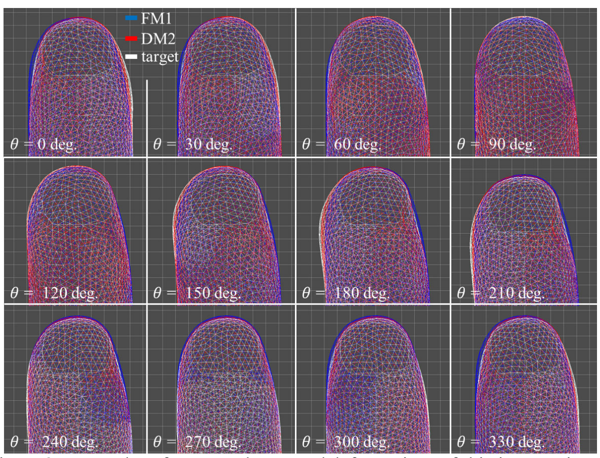

Figure 8. Examples of target and expected deformations of skin in Experiment 2. The deformation differed depending on the direction of motion θ.

screen. The force standards were determined by the subjects. For convenience of providing feedback, a circle centered on the origin of the vector was displayed on the answering screen.

C. Experimental Procedure

The experimental procedure was approved by the Ethics Review Board of the University of Electro-Communications (approval number: 20065). The experiment was carried out according to the following procedure:

(1) Experiment explanation:

The experimenter explained the purpose of the experiment and obtained consent for participation in the experiment. The purpose of the experiment was to investigate the difference in perception owing to the difference in the calculation method (i.e., rendering algorithm) in the presentation of the frictional force by the pin-array-type force feedback device.

(2) Preliminary questionnaire:

Subjects were asked to provide information regarding their attributes (i.e., age, gender, and dominant hand), VR experience, and haptic device experience.

(3) Measurement of finger elasticity:

The force correction coefficient α was calculated by the procedure described in Section IV.C and input into the experimental program.

(4) Explanation of experimental program operation:

The experimenter explained the operation for the experiment to the subjects. The presentation was started by pressing the space key. The subjects assessed the direction and intensity of the force acting on the finger. The subjects responded by drawing a vector on the screen with the mouse. In case of a mistake in the response, it was possible to return to the previous attempt by pressing the "n" key. The force acting on the finger included both compression and friction components. The subjects provided answers regarding the intensity of the force according to their own criteria.

(5) Attachment of device:

The device was attached to the right-hand index finger of the subject. The device was set so that the positional relationship between the finger and device was as close as possible to that depicted in Fig. 1.

(6) Practice 1:

Practice was performed for Experiment 1. First, the state of contact and friction between the finger and surface was explained while displaying the target deformation of the finger on the screen. Thereafter, the presentation and response were repeated until the subject became accustomed to the presentation and established the criteria for their response, or until the subject was satisfied. No feedback on the correct answer regarding the force direction was provided at this stage. No time limit was imposed for the practice.

(7) Experiment 1:

The subjects wore earplugs and noise-canceling headphones. All controls for the progress of the experiment were performed by the subjects, except when the subject required help. A break was provided during the experiment.

(8) Practice 2:

Practice for Experiment 2 was performed in the same manner as described in (6).

(9) Experiment 2:

Experiment 2 was performed in the same manner as described in (7).

(10) Post-questionnaire:

The subjects were asked to describe their impressions of the experiment freely.

VI. Results and Discussion

The results of Experiments 1 and 2 are discussed in this section. Ten subjects (mean age: 22.7, all male, all right-handed) participated in the experiment.

A. Experiment 1: Frictional Force

The results of Experiment 1 are discussed separately for the perception of the friction coefficient and the perception of the intensity. For the perception of the friction coefficient, first, the tangent/normal ratio k was obtained from the force vector answered by the subject. If correct perception occurred, k was expected to match the coefficient of friction μ. Fig. 9 presents the relationship between the coefficient of friction μ and perceived k. In this figure, the perceived k is plotted for each condition of depth d and friction direction (right/left). The tangent/normal ratio calculated from the x–z component of the sum of the forces of the target is also indicated by the dashed black line, which is labeled as "target." Furthermore, the tangent/normal ratios calculated from the x–z components of the sums of the forces presented in FM1 and DM2 are indicated by the dashed blue and red lines, respectively, which are labeled as "actual." In DM2, the ratio k tended to increase proportionally to the presented coefficient, whereas in FM1, it did not. The slope b of the regression line was tested for each condition (see t and p in Table I). In DM2, the difference between b and 0 was significant, whereas in FM1, no significant difference was observed. To confirm the difference between the algorithms, Welch's test was performed on the slopes of FM1 and DM2 under each condition (see t_1 and p_1 in Table I). The difference in the slope was significant under all conditions. The expected slope b was 1 when the friction coefficient was correctly perceived; however, DM2 exhibited a much larger slope. This is discussed later in this paper.

Fig. 10 presents the results of the perception of the force intensity. The intensity calculated from the x–z component of the sum of the target forces is indicated with a black dashed line, which is labeled as "target." Furthermore, the intensities calculated from the x–z component of each sum of the forces presented in FM1 and DM2 are indicated by dashed blue and red lines, respectively, which are labeled as "actual." Because the subjects decided the scale of the vector when answering, it was not possible to evaluate the perception of the absolute force intensity. Therefore, the vector length was normalized by dividing it by the average of the results obtained under all the conditions by a coefficient of friction $\mu = 0$ for each subject. The mean and standard deviations of the plot were calculated for this normalized intensity. Therefore, this plot was obtained for observing the qualitative tendency of the presented force and perceived force with the change in the coefficient of friction

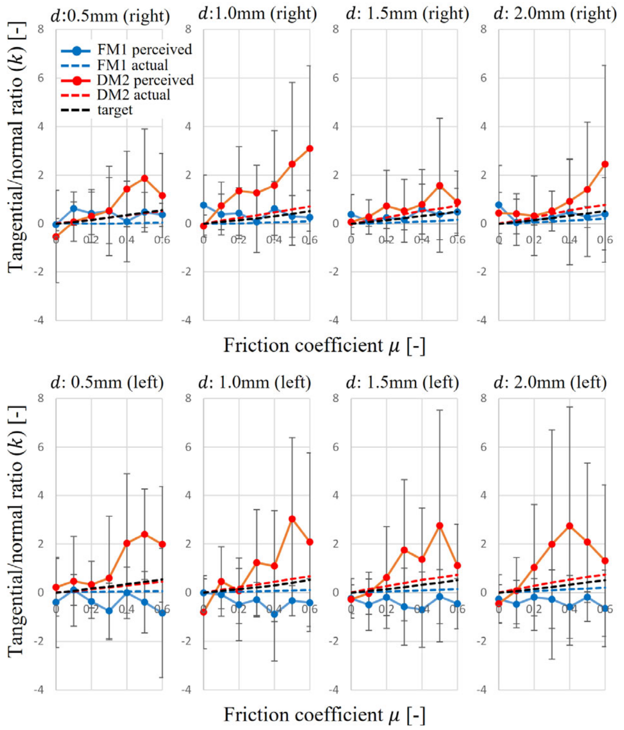

Fig. 9. Relationship between friction coefficient μ and tangent/normal ratio k. In DM2, k tended to increase proportionally to μ, whereas in FM1, it did not.

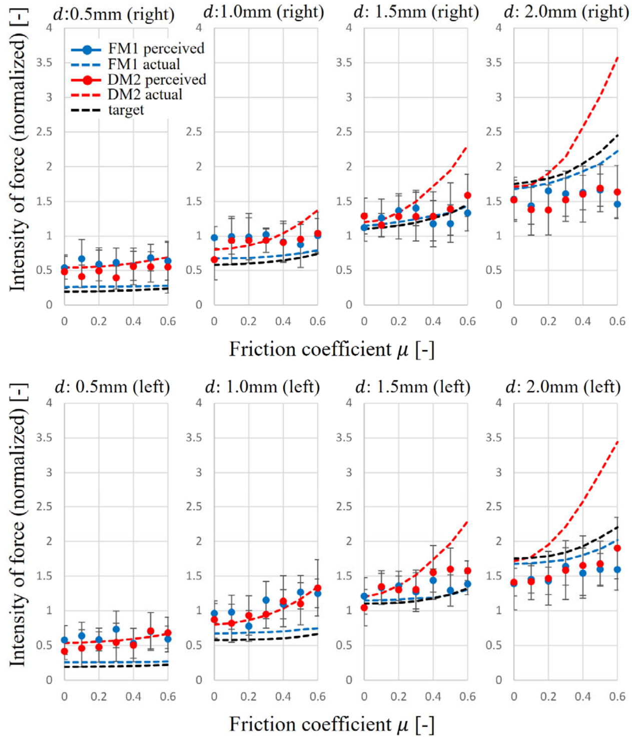

Fig. 10. Relationship between friction coefficient μ and normalized intensity of perceived force. In DM2, the actual force was considerably larger than the target, but the perceived force appeared not to be particularly large.

TABLE I
STATISTICAL ANALYSIS OF SLOPE OF k/μ. SIGNIFICANT DIFFERENCES IN THE SLOPES OF FM1 AND DM2 WERE OBSERVED.

	right		left	
d = 0.5 mm	**FM1**	**DM2**	**FM1**	**DM2**
$b \pm \sigma$	0.209±0.644	3.496±0.917	-0.698±0.869	3.88±1.206
t	0.324	3.813	-0.804	3.217
p	0.747	<0.001**	0.424	0.002**
v	122.0		123.6	
t_1	-14.6		-15.3	
p_1	<0.001**		<0.001**	
d = 1.0 mm	**FM1**	**DM2**	**FM1**	**DM2**
$b \pm \sigma$	-0.532±1.117	4.734±4.533	-0.752±1.168	5.292±5.691
t	-0.842	3.721	-1.164	3.712
p	0.403	<0.001**	0.248	<0.001**
v	99.6		94.8	
t_1	-18.4		-19.2	
p_1	<0.001**		<0.001**	
d = 1.5 mm	**FM1**	**DM2**	**FM1**	**DM2**
$b \pm \sigma$	0.436±0.575	1.821±2.153	-0.174±1.298	3.735±6.215
t	0.963	2.077	-0.255	2.507
p	0.339	0.042*	0.799	0.015*
v	101.9		95.2	
t_1	-7.0		-11.8	
p_1	<0.001**		<0.001**	
d = 2.0 mm	**FM1**	**DM2**	**FM1**	**DM2**
$b \pm \sigma$	-0.126±1.489	3.084±4.362	-0.352±1.11	3.922±10.549
t	-0.173	2.471	-0.559	2.021
p	0.863	0.016*	0.578	0.047*
v	109.6		82.1	
t_1	-11		-10.4	
p_1	<0.001**		<0.001**	

μ. In both the FM1 and DM2 algorithms, there was no constraint to match the sum of the forces with the target, and the value could differ from the target. In DM2, the acting force was considerably larger than the target in terms of the sum of the acting forces; however, the force was not perceived to be particularly large by the subject.

B. Experiment 2: Direction of Frictional Force

The results of Experiment 2 are discussed separately for the perception of the friction direction and the perception of the intensity. First, for the friction direction, Fig. 11 presents a plot of the perceived direction with respect to the presented direction θ. In this figure, the direction of the force calculated in contact with the target in the x–y plane is indicated by a black dashed line, which is labeled as "target." The directions calculated from the sum of the forces determined by FM1 and DM2 are also plotted with dashed blue and red lines, respectively, which are labeled as "actual." In both FM1 and DM2, a region existed around 270° in which the direction could not be correctly expressed as the total force vector owing to the orientation of the device pin and the posture of wearing it on the finger. Because FM1 and DM2 find the optimum output under this constraint, the resulting force does not have the component in this direction, and the direction of total force (i.e. actual) in Figure 12 is discontinuous around 270°. For each condition of FM1 and DM2, there was no error bias across all presentation angles (FM1: t = 0.315, p = 0.753; DM2: t = -0.006, p = 0.995). However, several significant deviations from the target angle depending on the azimuth were observed, which are indicated by asterisks in Fig. 11. When comparing the variance

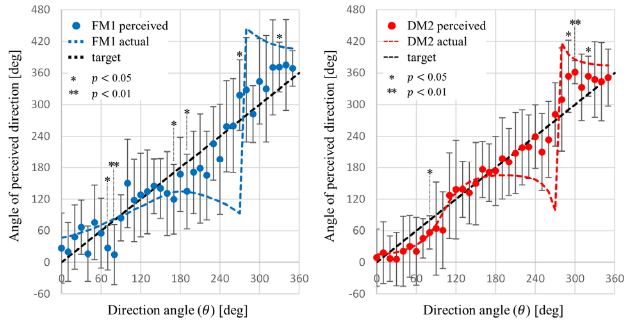

Fig. 11. Relationship between presented and perceived angles of frictional motion. Significant deviations from the target are marked with asterisks.

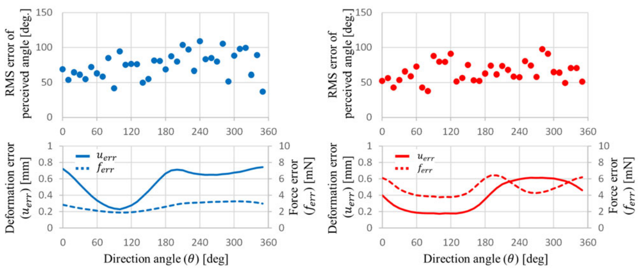

Fig. 12. RMS error of perceived direction and deformation/force errors depending on target angle. No significant correlation was observed, except for a weak correlation between the RMS error and f_{err} in FM1.

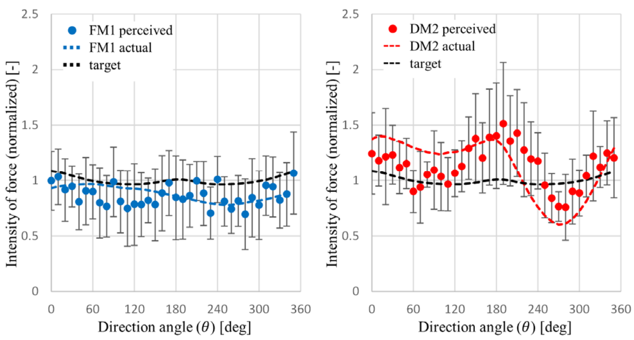

Fig. 13. Normalized intensity of perceived force depending on target angle. A significant correlation between the actual and perceived forces was observed in DM2.

of the error across all angles between FM1 and DM2, it was observed that the variance of FM1 was significantly larger than that of DM2 ($F = 1.348, p = 0.0024$). To clarify the effect of the matching error on the perception, the root-mean-square (RMS) error in the friction direction and the matching error due to FM1 and DM2 (u_{err}, f_{err}) are depicted in Fig. 12. A correlation analysis was performed for each RMS error and matching error. No significant correlation was observed, except for a weak correlation with the force matching error f_{err} for FM1 ($r = 0.371, t = 2.330, p = 0.026$).

Fig. 13 depicts the results on the perception of the force intensity. The plot indicates the intensity calculated from the x–y component of the sum of the target forces with a black dashed line, which is labeled as "target." Furthermore, the intensity calculated from the x–y components of the sums of the forces presented in FM1 and DM2 are indicated by the dashed blue and red lines, respectively, which are labeled as "actual." As in Experiment 1, because the criteria for answering were decided by the subjects, it was not possible to evaluate the perception of the absolute force intensity. Therefore, the force intensity was normalized by division by the average of the results for all angle conditions for each subject. The mean and standard deviation of the plot were calculated for this normalized intensity. In DM2, the change in the presentation force with the angle was relatively large, which appeared to affect the perception of the subjects. A significant correlation between the two was observed for DM2 ($r = 0.585, t = 4.213, p < 0.01$).

C. Discussion

In Experiment 1, it was found that the friction coefficient was difficult to perceive with FM1, whereas this was possible with DM2. However, the recognized tangent/normal ratio k was much larger than the presented coefficient of friction μ. Although the reason cannot be clarified from this experiment, possible factors include problems with the algorithm, device characteristics, human perceptual characteristics, and the influence of the response method in the experiment. Further investigation is required in future experiments. Another concern regarding this result is that in DM2, the perceptual disturbance appeared to increase near the friction coefficient $\mu = 0.6$. As the friction coefficient increased, the skin underwent greater shear deformation. One possible reason for the disturbance is the difficulty of causing large deformations by the device used in the experiment. As stated previously, the orientation of the device pins was almost perpendicular to the skin surface, and a small tangential force was applied. Intuitively, it is difficult and inefficient for shear deformation to be caused by the distribution of normal forces. This notion may lead us to designing a device with different pin configurations that is optimal for the DM algorithm. Regarding the perception of the force intensity, the output force of DM2 was considerably different from that of the target, but the subject perception was not significantly affected. The results suggest that tactile sensation, without the sensation of force that is derived from bathyesthesia, does not provide accurate information of the force as a sum on the skin surface.

In Experiment 2, it was revealed that the perception of the friction direction was possible with both FM1 and DM2 to a certain extent, but DM2 provided better perception accuracy than FM1. Both FM1 and DM2 exhibited large variability near azimuths of 90 and 270°. This is considered to be due to the influence of the device pin orientation. As described in Section IV.B, the pins were arranged on the cylindrical surface and the direction of the pin operation was the normal direction of the cylindrical surface. Because the device was mounted at an angle to the friction surface, the component in the 90° (y+) direction could be expressed even though it was small. However, the component in the direction around 270° (y-) could not be expressed in principle. This is considered to have made the perception at this angle particularly unstable.

Interestingly, this direction was also recognized in FM1. The result that the direction could be perceived by FM1 is intuitively inconsistent with the result that it was difficult to recognize the tangent/normal ratio in Experiment 1. Further investigation is required to elucidate the cause, but one possibility is that the clues to which the subject paid attention changed owing to the difference in the tasks. As the task of Experiment 2 included the informational element of direction selection, it is possible that the subject considered mapping from the stimulus to the direction by using a method that is not simply physical.

VII. Conclusion

We have presented a rendering method that considers the constraints for multipoint tactile displays. We proposed and formulated a deformation matching method that calculates the output force to minimize the error between the target skin deformation and skin deformation owing to the device action. As a generalization of the conventional method, we also formulated a force matching method that minimizes the force error.

To compare the perceptual characteristics of subjects by deformation matching and force matching, surveys of the perception of the friction coefficient and of the perception of the friction direction were performed in Experiments 1 and 2, respectively. The results demonstrated that the perception of the friction coefficient was more sensitive in DM2 than in FM1 and that the recognition of the friction direction was more accurate in DM2 than in FM1. The effectiveness of deformation matching in the friction expression was confirmed based on these results.

The experimental results are considered to be meaningful in terms of the comparison between FM1 and DM2, but further studies are required to elucidate the human perceptual characteristics. The reason that the perception of the tangent/normal ratio was much larger than that of the friction coefficient in the simulation needs to be clarified through an evaluation of the perceptual characteristics using real objects and experiments, with devices that have different DoF.

A linear FEM was used to model the finger as the first step of the study. In reality, the skin tissue is nonlinear and nonuniform. Moreover, in the model of the action by the pin, it was assumed that the pin and skin surface did not slip, but in reality, slipping may occur and the point of action on the skin can be changed. Furthermore, the interference between the base and the finger and contact between the fastener and the finger were not considered. It is expected that a more accurate tactile presentation will be possible by using a model that considers these factors.

In this study, we used an approach to minimize the displacement error. From the perspective of considering the human stimulus perception mechanism, as opposed to optimization by deformation, optimization by strain energy density weighted on the region where the receptors are distributed will be an interesting topic. In such a formulation, it will be necessary to discuss whether the convergence of the solution search is guaranteed mathematically.

Real-time processing of the calculations was not included in this study. It is quite difficult to solve nonlinear programming problems in real time, but we are beginning to study the acceleration of processing using a GPU. Moreover, we are optimistic about future advances in computers and consider that optimization problems, for example, will be calculated efficiently by quantum computers.

Within the scope of this study, the experimental task was limited to the perception of friction. A further advantage of the use of multi-DoF haptic devices is expected to be the representation of complex shapes. Thus, it is necessary to evaluate the effect of the proposed method on shape recognition tasks.

References

[1] I. Sarakoglou, N. Garcia-Hernandez, N. G. Tsagarakis, and D. G. Caldwell, “A high performance tactile feedback display and its integration in teleoperation,” *IEEE Trans. Haptics*, vol. 5, pp. 252–263, May 2012, DOI: 10.1109/toh.2012.20.

[2] Y. Ujitoko, T. Taniguchi, S. Sakurai, and K. Hirota, “Development of finger-mounted high-density pin-array haptic display,” *IEEE Access*, vol. 8, pp. 145107–145114, Aug. 2020, DOI: https://doi.org/10.1109/ACCESS.2020.3015058.

[3] S.-C. Kim, C.-H. Kim, G.-H. Yang, T.-H. Yang, B.-K. Han, S.-C. Kang, and D.-S. Kwon, “Small and lightweight tactile display(SaLT) and its application,” in *Proc. WHC*, Salt Lake City, UT, USA, 2009, pp. 69–74.

[4] K.-U. Kyung and J.-Y. Lee, “Ubi-pen: A haptic interface with texture and vibrotactile display,” *IEEE Comput. Graph. Appl.*, vol. 29, no. 1, pp. 56–64, Jan.–Feb. 2009.

[5] A. G. Perez, D. Lobo, F. Chinello, G. Cirio, M. Malvezzi, J. S. Martín, D. Prattichizzo, and M. A. Otaduy, “Optimization-based wearable tactile rendering,” *IEEE Trans. Haptics*, vol. 10, no. 2, pp. 254–264, Apr.–Jun. 2017.

[6] M. Verschoor, D. Casas, and M. A. Otaduy, “Tactile rendering based on skin stress optimization,” *ACM Trans. Graph.*, vol. 39, no. 4, Jul. 2020, Art. no. 90.

[7] A. G. Perez, G. Cirio, F. Hernandez, C. Garre, and M. A. Otaduy, “Strain limiting for soft finger contact simulation,” in *Proc. WHC*, Daejeon, Korea (South), 2013, pp. 79–84.

[8] T. H. Massie and J. K. Salisbury, “The PHANTOM haptic interface: A device for probing virtual objects,” in *Proc. ASME Winter Annual Meeting, Symposium on Haptic Interfaces for Virtual Environment and Teleoperator Systems*, Chicago, IL, USA, 1994, pp. 295–300.

[9] K. Minamizawa, H. Kajimoto, N. Kawakami, and S. Tachi, “A wearable haptic display to present the gravity sensation - preliminary observations and device design,” in *Proc. WHC*, Tsukuba, Japan, 2007, pp. 133–138.

[10] M. Konyo, S. Tadokoro, and T. Takamori, “Artificial tactile feel display using soft gel actuators,” in *Proc. IEEE ICRA*, San Francisco, CA, USA, 2000, pp. 3416–3421, DOI: 10.1109/ROBOT.2000.845250.

[11] T.-H. Yang, S.-Y. Kim, C. H. Kim, D.-S. Kwon, and W. J. Book, “Development of a miniature pin-array tactile module using elastic and electromagnetic force for mobile devices,” in *Proc. WHC*, Salt Lake City, UT, USA, 2009, pp. 13–17, DOI: 10.1109/WHC.2009.4810818.

[12] T. Nojima, Y. Ooide, and H. Kawaguchi, “Hairlytop interface: An interactive surface display comprised of hair-like soft actuators,” in *Proc. WHC*, Daejeon, Korea (South), 2013, pp. 431–435.

[13] A. Frisoli, M. Solazzi, F. Salsedo, and M. Bergamasco, “A fingertip haptic display for improving curvature discrimination,” *Presence*, vol. 17, no. 6, pp. 550–561, Dec. 2008.

[14] A. L. Guinan, M. N. Montandon, A. J. Doxon, and W. R. Provancher, “Discrimination thresholds for communicating rotational inertia and torque using differential skin stretch feedback in virtual environments,” in *Proc. IEEE Haptics Symp.*, Houston, TX, USA, 2014, pp. 277–282.

[15] Z. F. Quek, S. B. Schorr, I. Nisky, W. R. Provancher, and A. M. Okamura, “Sensory substitution using 3-degree-of-freedom tangential and normal skin deformation feedback,” in *Proc. IEEE Haptics Symp.,* Houston, TX, USA, 2014, pp. 27–33.

[16] S. Yazdian, A. J. Doxon, D. E. Johnson, H. Z. Tan, and W. R. Provancher, “Compliance display using a tilting-plate tactile feedback device,” in *Proc. IEEE Haptics Symp.*, Houston, TX, USA, 2014, pp. 13–18.

[17] J. C. Bliss, M. H. Katcher, C. H. Rogers, and R. P. Shepard, “Optical-to-tactile image conversion for the blind,” IEEE Trans. Man Mach. Syst., vol. 11, no. 1, pp. 58–65, Mar. 1970.

[18] Y. Ikei, K. Wakamatsu, and S. Fukuda, “Vibratory tactile display of image-based textures,” IEEE Comput. Graph. Appl., vol. 17, no. 6, pp. 53–61, Nov./Dec. 1997.

[19] H. Kajimoto, N. Kawakami, T. Maeda, and S. Tachi, “Tactile feeling display using functional electrical stimulation,” in *Proc. ICAT*, 1999, pp. 107–114.

[20] K. Salisbury, D. Brock, T. Massie, N. Swarup, and C. Zilles, “Haptic rendering: Programming touch interaction with virtual objects,” in *Proc. Symposium on Interactive 3D Graphics*, Monterey, CA, USA, 1995, pp. 123–130.

[21] C. B. Zilles and J. K. Salisbury, “A constraint-based god object method for haptic display,” in *Proc. IEEE IROS*, Pittsburgh, PA, USA, 1995, pp. 145–151.

[22] H. B. Morgenbesser and M. A. Srinivasan, “Force shading for haptic shape perception,” in *Proc. ASME Dynamic Systems and Control Division*, Atlanta, GA, USA, 1996, vol. 58, pp. 407–412.

[23] M. Minsky, O. Ming, O. Steele, F. P. Brooks, and M. Behensky, “Feeling and seeing: issues in force display,” in *Proc. Symposium on Interactive 3D Graphics*, Snowbird, UT, USA, 1990, pp. 235–241.

[24] F. Barbagli, A. Frisoli, K. Salisbury, and M. Bergamasco, “Simulating human fingers: a soft finger proxy model and algorithm,” in *Proc. HAPTICS*, Chicago, IL, USA, 2004, pp. 9–17.

[25] M. Ciocarlie, C. Lackner, and P. Allen, “Soft finger model with adaptive contact geometry for grasping and manipulation tasks,” in *Proc. WHC*, Tsukuba, Japan, 2007, pp. 219–224.

[26] C. Duriez, H. Courtecuisse, J.-P. de la Plata Alcalde, and P. -J. Bensoussan, “Contact skinning,” in *Proc. Eurographics*, Crete, Greece, 2008, pp. 313–320.

[27] A. Talvas, M. Marchal, C. Duriez, and M. A. Otaduy, “Aggregate constraints for virtual manipulation with soft fingers,” *Trans. Vis. Comput. Graph.*, vol. 21, no. 4, pp. 452–461, Apr. 2015.

[28] J. Jacobs and B. Froehlich, “A soft hand model for physically-based manipulation of virtual objects,” in *Proc. IEEE VR*, Singapore, 2011, pp. 11–18.

[29] C. Garre, F. Hernandez, A. Gracia, and M. A. Otaduy, “Interactive simulation of a deformable hand for haptic rendering,” in *Proc. WHC*, Istanbul, Turkey, 2011, pp. 239–244.

[30] K. Hirota and K. Tagawa, “Interaction with virtual object using deformable hand,” in *Proc. IEEE VR*, Greenville, SC, USA, 2016, pp. 49–56.

[31] K. Sato, H. Nii, N. Kawakami, and S. Tachi, “Electrotactile stimulation based on strain energy density of the fingertip,” in *Proc. EuroHaptics*, Madrid, Spain, 2008, pp. 724–729.

[32] D. Maemori, L. B. Porquis, M. Konyo, and S. Tadokoro, "A Multi-DOF Haptic Representation Using Suction Pressure Stimuli on Finger Pads," in *Proc. Eurographics*, Crete, Greece, 2014, pp. 285-294.

[33] H. Barreiro, S. Sinclair, and M. A. Otaduy, "Ultrasound Rendering of Tactile Interaction with Fluids," In *Proc. World Haptics Conf.*, Tokyo, JAPAN, 2019, pp. 521-526.

[34] H. Barreiro, S. Sinclair, and M. A. Otaduy, "Path Routing Optimization for STM Ultrasound Rendering," *IEEE Trans. Haptics*, vol. 13, no. 1, pp. 45-51, Jan.-March 2020.

[35] S. Weinstein, “Intensive and extensive aspects of tactile sensitivity as a function of body part, sex, and laterality,” in *Proc. First International Symposium on the Skin Senses*, Tallahassee, FL, USA, 1968.

[36] J. M. Loomis and C. C. Collins, “Sensitivity to shifts of a point stimulus: An instance of tactile hyperacuity,” *Percept. Psychophys.*, vol. 24, no. 6, pp. 487–492, Dec. 1978.

[37] M. Nakatani, H. Kajimoto, N. Kawakami, and S. Tachi, “Tactile sensation with high-density pin-matrix,” in *Proc. APGV*, A Coruña, Spain, 2005, pp. 169–169.

[38] J. H. Kirman, “Tactile apparent movement: The effects of interstimulus onset interval and stimulus duration,” *Percept. Psychophys.*, vol. 15, no. 1–6, Jan. 1974, DOI: https://doi.org/10.3758/BF03205819.

[39] M. A. Srinivasan and K. Dandekar, “An investigation of the mechanics of tactile sense using two-dimensional models of the primate fingertip,” *J. Biomech. Eng.*, vol. 118, no. 1, pp. 48–55, Feb. 1996.

[40] K. Kobayashi and T. Maeno, “Relationship between the structure of finger tissue and the location of tactile receptors (2nd report, method of dynamic contact analysis and results for contact between the finger and plane plate),” *Trans. JSME*, vol. 64, no. 628, pp. 4798–4805, 1998 (in Japanese).

[41] Y. Makino, N. Asamura, and H. Shinoda, “A whole palm tactile display using suction pressure,” in *Proc. IEEE ICRA*, New Orleans, LA, USA, 2004, pp. 1524–1529.

[42] O. C. Zienkiewicz, R. L. Taylor, and J. Z. Zhu, *The Finite Element Method: Its Basis and Fundamentals*, 7th ed., Elsevier Ltd., 2013.

[43] N. Yamashita, *Nonlinear programming*, Application optimization series No.6, Asakura Publishing Co., Ltd., 2015 (in Japanese).

[44] N. Mitsuhashi, K. Fujieda, T. Tamura, S. Kawamoto, T. Takagi, and K. Okubo, “BodyParts3D: 3D structure database for anatomical concepts,” *Nucleic Acids Res.*, vol. 37, Database issue, pp. D782–D785, Jan. 2009, DOI: 10.1093/nar/gkn613.

[45] S. Yoshimura, R. Shioya, H. Noguchi, and T. Miyamura, “Advanced general-purpose computational mechanics system for large-scale analysis and design,” *J. Computat. Appl. Math.*, vol. 149, no. 1, pp. 279–296, Dec. 2002.

Koichi Hirota received his B.S. and Ph.D. degrees from the University of Tokyo, Tokyo, Japan, in 1988 and 1994, respectively. He then became an Assistant Professor at Toyohashi University of Technology, Toyohashi, Japan, in 1995. In 2000, he became an Associate Professor at the University of Tokyo. He is currently a Professor at the Department of Informatics, Graduate School of Informatics and Engineering, University of Electro-Communications, Tokyo. His research interests include haptic devices, haptic rendering, and human–computer interaction.

Yusuke Ujitoko received his B.E. degree in mechanical engineering and M.A.E. degree in interdisciplinary information studies from the University of Tokyo, Tokyo, Japan, in 2014 and 2016, respectively. He received his Ph.D. degree from the University of Electro-Communications, Tokyo, Japan, in 2020. He was a Researcher at Hitachi, Ltd., Tokyo, by 2020, and is currently a Researcher at the NTT Communication Science Laboratories. His research interests include applied haptic perception and haptic interfaces.

Sho Sakurai received her B.E. degree in social and information studies from Gunma University, Maebashi, Japan, in 2007, and M.A.E. degree in interdisciplinary information studies and Ph.D. degree in engineering, from the University of Tokyo, Tokyo, Japan, in 2010 and 2014, respectively. He is currently a Project Assistant Professor at the Graduate School of Information Systems, the University of Electro-Communications, Tokyo. Her research interests are multi-modal/cross-modal interfaces and human–computer interaction. She is also active as a manga artist for the introduction of the latest research on virtual reality and artificial intelligence.

Takuya Nojima received his Ph.D. degree from the University of Tokyo, Tokyo, Japan, in 1988. He was a researcher at the Japan Aerospace Exploration Agency in December 2008 and is currently an associate professor with the Department of Informatics, Graduate School of Informatics and Engineering, University of Electro-Communications. He was a Visiting Associate Professor at the Massachusetts Institute of Technology Media Lab from August 2015 to March 2016. His research interests include augmented sports, entertainment computing, and haptic and tangible interfaces.